DOI: 10.17617/2.3186650
Proceedings of the 9th Solar Polarization Workshop SPW9
A workshop held in Göttingen, Germany, from August 26 to August 30, 2019
Achim Gandorfer, Andreas Lagg, Kerstin Raab (eds.)

Resonance Line Polarization in Spherically Symmetric Moving Media: a Parametric Study

A. Megha,[1,*] M. Sampoorna,[1] K. N. Nagendra,[1,2], L. S. Anusha,[3] and K. Sankarasubramanian[1,4,5]

[1]Indian Institute of Astrophysics, Koramangala, Bengaluru, India

[2]Istituto Ricerche Solari Locarno, Locarno Monti, Switzerland

[3]Max-Planck-Institut für Sonnensystemforschung, Göttingen, Germany

[4]Space Astronomy Group, U. R. Rao Satellite Centre, ISITE Campus, Bengaluru

[5]CESSI, IISER, Kolkata, India

[*]*Email:* megha@iiap.res.in

Abstract. In the present paper we consider the problem of resonance line polarization formed in the spherically symmetric expanding atmospheres. For the solution of the concerned polarized transfer equation we use the comoving frame formulation, and apply the Accelerated Lambda Iteration (ALI) method. We restrict ourselves to the non-relativistic regime of velocities wherein mainly Doppler shift effects are significant. For our studies, we consider the scattering on a two-level atom, including the effects of partial frequency redistribution (PFR). We present the dependence of linearly polarized profiles on different atmospheric and atomic parameters.

1 Introduction

The spectroscopic observations of different classes of astrophysical objects like supergiants, Wolf-Rayet stars, novae, and supernovae indicate the existence of high-velocity outward gas flows. The spectral line profiles of these objects are of P Cygni type (Beals 1931) with redshifted emission and blueshifted absorption indicating the rapid outflow of matter in the outer layers of their atmospheres. These outward gas flows lead to extended atmospheres. Even small extensions present in solar type stars are highly structured which give rise to significant observable effects. Therefore a precise treatment of such problems require going beyond the plane-parallel model.

The detailed discussions on techniques for solving the problem of line formation in extended and expanding atmospheres in both observer's frame and comoving frame (CMF) are described in Hubeny & Mihalas (2014, and references therein). These earlier works considered only the intensity profiles accounting for either complete frequency redistribution (CFR) or PFR in scattering. In Megha et al. (2019), we extended this problem to include the resonance line polarization. To this end we extended CMF-ALI method of Hauschildt & Baron (2004) to include polarization and PFR. For our studies we considered the CMF transfer equation in the non-relativistic limit (i.e., the advection and aberration terms were

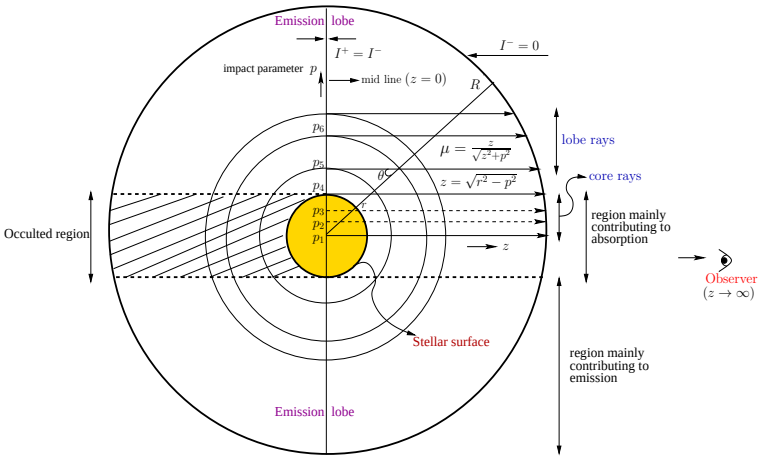

Figure 1. The (p, z) representation used to solve the spherically symmetric radiative transfer equation.

excluded and only Doppler shift effects were retained). Here we use the CMF-PALI method presented in Megha et al. (2019) to understand the quantitative behavior of the linear polarization when the basic model parameters are varied systematically one at a time keeping the other parameters as constants.

2 The comoving frame polarized transfer equation

In order to effectively treat the outward peaking of the radiation field in a spherically symmetric atmosphere, we consider the transfer equation in (p, z) representation (Hummer & Rybicki 1971), where p is the impact parameter of the ray and z is the distance measured along it (see Figure 1). In this representation, the polarized CMF transfer equation, under the non-relativistic limit is given by

$$\pm \frac{\partial \boldsymbol{I}^{\pm}(z,p,x)}{\partial \tau(z,x)} = \boldsymbol{I}^{\pm}(z,p,x) - \boldsymbol{\mathcal{S}}(z,x) + \frac{a(r,p)}{\chi(r,x)} \frac{\partial \boldsymbol{I}^{\pm}(z,p,x)}{\partial x}, \tag{1}$$

where + and − stand for outgoing and incoming rays respectively, $\boldsymbol{I}^{\pm} = [I_0^{0,\pm}, I_0^{2,\pm}]^{\mathrm{T}}$ is a 2-component irreducible specific intensity vector (Frisch 2007), and $x = (\nu - \nu_0)/\Delta\nu_{\mathrm{D}}$ (with ν_0 being the line center frequency and $\Delta\nu_{\mathrm{D}}$ the Doppler width). The monochromatic optical depth along the tangent ray is defined as $d\tau = [\varphi(x) + \beta_c]d\tau_r/\mu$ (with r being the radial distance), where $d\tau_r = -\chi_l(r)dr$ is the radial optical depth with $\chi_l(r)$ being the line averaged absorption coefficient, $\mu(r,p) = \sqrt{1-(p^2/r^2)}$, and $\beta_c = \chi_c(r)/\chi_l(r)$ with $\chi_c(r)$ being the continuum absorption coefficient. The total absorption coefficient $\chi(r,x) = \chi_l(r)\varphi(x) + \chi_c(r)$, where the line absorption profile function $\varphi(x)$=$H(a,x)$ is a Voigt function, with a the damping parameter. In the CMF, $\varphi(x)$ is angle-independent. All the effects of the velocity field are contained in the last term of Equation (1), wherein

$$a(r,p) = (1-\mu^2)\frac{V}{r} + \mu^2 \frac{dV}{dr}. \tag{2}$$

Here $V = v_r/v_{\rm th}$ is the non-dimensional velocity, with v_r the radial velocity and $v_{\rm th}$ the thermal velocity. The CMF total source vector is given by

$$\boldsymbol{\mathcal{S}}(z,x) = \frac{\varphi(x)\boldsymbol{\mathcal{S}}_l(z,x) + \beta_c \boldsymbol{\mathcal{S}}_c}{\varphi(x) + \beta_c}, \tag{3}$$

where the unpolarized continuum source vector $\boldsymbol{\mathcal{S}}_c = B_{\nu_0}\boldsymbol{\mathcal{U}}$, with B_{ν_0} the Planck function at the line center, and $\boldsymbol{\mathcal{U}} = (1,0)^{\rm T}$. For a two-level atom with infinitely sharp and unpolarized lower level, the line source vector has the form

$$\boldsymbol{\mathcal{S}}_l(z,x) = \epsilon B_{\nu_0}\boldsymbol{\mathcal{U}} + \int_{-\infty}^{+\infty} dx' \frac{1}{2} \int_{-1}^{+1} d\mu' \frac{\boldsymbol{\mathcal{R}}(x,x')}{\varphi(x)} \boldsymbol{\Psi}(\mu')\boldsymbol{\mathcal{I}}(\tau,\mu',x'). \tag{4}$$

Here ϵ is the thermalization parameter, $\boldsymbol{\mathcal{R}}$ the 2×2 non-magnetic angle-averaged PFR matrix (Bommier 1997), and $\boldsymbol{\Psi}$ the Rayleigh phase matrix in the irreducible basis (Frisch 2007).

We solve Equation (1) by applying the polarized ALI method (see, e.g., the reviews by Nagendra 2003, 2014). The details of this method are discussed in Megha et al. (2019). Hence we do not repeat them here.

3 Model parameterization

For our studies we consider the following set of 'standard model parameters'. An isothermal, spherically symmetric atmosphere with inverse square law opacity distribution (i.e., $\chi_{l,c} \propto r^{-n}$, here the power law opacity index n=2), a frequency averaged total radial line optical thickness of T, and an outer radius R is considered. We use reflecting boundary condition, namely $\boldsymbol{\mathcal{I}}^+(\tau = T, p, x) = \boldsymbol{\mathcal{I}}^-(\tau = T, p, x)$ at the lower boundary and $\boldsymbol{\mathcal{I}}^-(\tau = 0, p, x) = 0$ at the outer boundary. For discretization of radius r, the impact parameter p, angle μ, frequency x, and depth grid τ_r we have followed Anusha et al. (2009). The 'standard model parameters' are: $T = 10^6$, $R = 30$, $\beta_c = 10^{-6}$, $\epsilon = 10^{-4}$, $a = 10^{-3}$, $B_{\nu_0} = 1$, and no elastic collisions. For our studies we consider both static ($V(r)$=0) and a constantly moving atmosphere with $V(r)$=3. We show all the results for a fixed line-of-sight of μ=0.11. The effects of extendedness R and the elastic collisions on the linearly polarized line profiles formed in static media and in the presence of velocity fields are presented in Megha et al. (2019). Following Nagendra (1988, 1994, 1995) here we present the dependence of linearly polarized profiles on a, ϵ, β_c, T, and the power law opacity index n, when they are varied one at a time around the standard model parameters, while keeping the other parameters as constants.

4 Results and discussions

4.1 Dependence on thermalization parameter ϵ

Figure 2 shows the emergent PFR (I, Q/I) profiles from a spherically symmetric static (panel a) and a constantly moving atmosphere with $V(r)$=3 (panel b) for varying values of thermalization parameter ϵ in the range [10^{-8}, 1]. ϵ gives the probability that a photon is destroyed during scattering process due to collisional de-excitation. Here ϵ=1 refers to pure LTE case

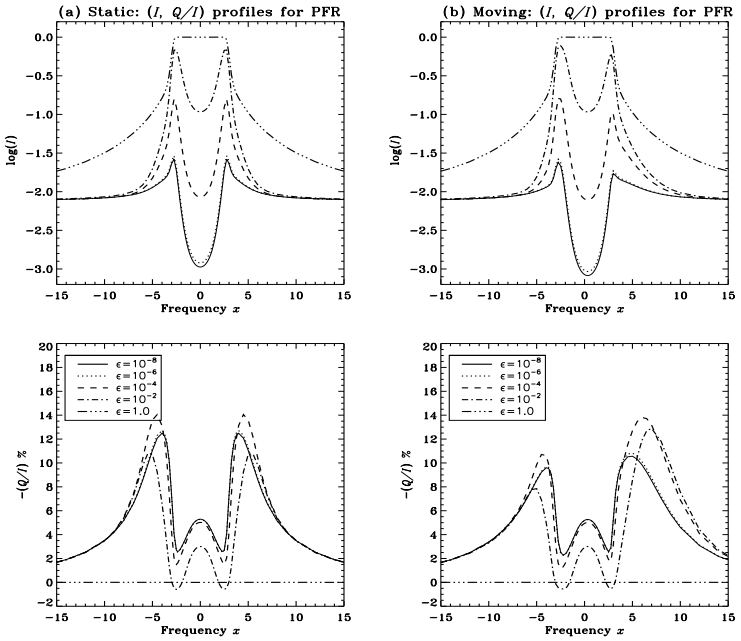

Figure 2. Emergent PFR $(I, Q/I)$ profiles from a spherically symmetric static (panel a) and a constantly moving atmosphere with $V(r)$=3 (panel b) for varying values of thermalization parameter ϵ (which are given in the inset box).

and other values refer to non-LTE case. As the value of ϵ increases from 10^{-8} to 1, the thermal coupling of photons with the continuum also increases due to increase in the number of collisions in the medium. For $\epsilon = 10^{-8}$, the intensity shows a self-absorbed symmetric emission profile for the static case (see Figure 2a). As the ϵ value increases from 10^{-8} to 1, the intensity around the line core region increases. Also self-absorbed part of the profile becomes shallower and finally disappears for $\epsilon = 1$. Furthermore for $\epsilon = 1$, the symmetric emission peaks around $x = \pm 2.25$ disappear as there is no scattering contribution from the extended lobes. The polarization profile (Figure 2a, lower panel) for $\epsilon = 10^{-8}$ shows a triple peak structure due to PFR. As ϵ value increases, the magnitude of polarization in the line core region decreases due to a decrease in the number of scatterings and the profile becomes completely flat with zero polarization for $\epsilon = 1$. However at the PFR wing peaks, we see that Q/I is nearly the same for ϵ between 10^{-8} and 10^{-6}, then increases for $10^{-5} \leq \epsilon \leq 10^{-4}$, and then decreases for $\epsilon \geq 10^{-3}$. To understand this we recall that in a spherical atmosphere with $B_{\nu_0} = 1$ photons are created substantially closer to the surface (see Kunasz & Hummer 1974), from where they escape much more readily. With increase in ϵ the photon creation rate increases while mean number of scatterings decrease. For $\epsilon \leq 10^{-6}$, mean number of scatterings are nearly the same (see Table IV of Kunasz & Hummer 1974 which corresponds to the case of $n = 0$) so that I and Q/I are nearly the same for ϵ between 10^{-8} and 10^{-6}. For $10^{-5} \leq \epsilon \leq 10^{-4}$, although the mean number of scatterings decrease relatively, since the

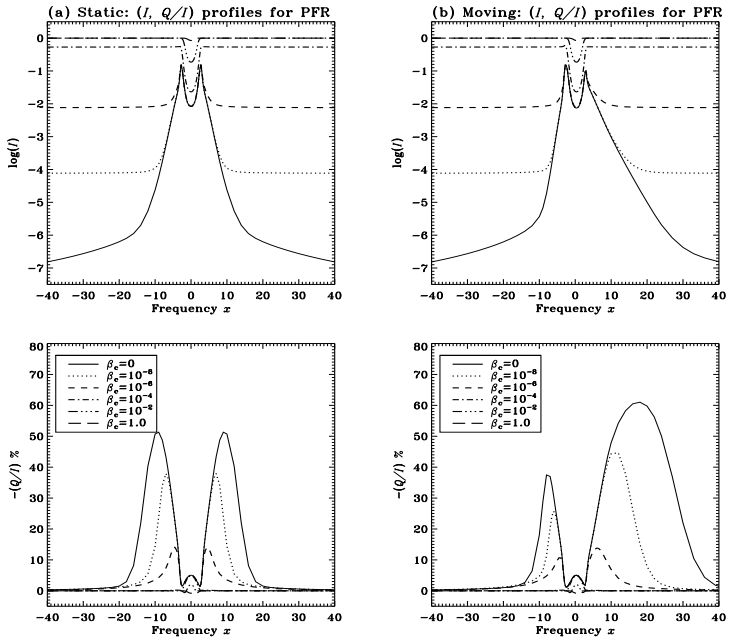

Figure 3. Emergent PFR $(I, Q/I)$ profiles from a spherically symmetric static (panel a) and a constantly moving atmosphere with $V(r)$=3 (panel b) for varying values of continuous absorption co-efficient β_c (which are given in the inset box).

photons are created near the surface a moderate number of scatterings would result in larger values of Q/I. This is particularly the case for highly extended atmosphere ($R = 30$) considered in this paper. For $\epsilon > 10^{-4}$ mean number of scatterings decrease considerably resulting in decreasing values of Q/I as in planar atmospheres. Our numerical studies show that, such a dependence of Q/I on ϵ is seen for $R > 10$, while for $R \leq 10$ the Q/I monotonically decreases with increasing ϵ not only in the line core but also in the PFR wings.

In the presence of velocity fields the line profiles are asymmetric about the line center (see Figure 2b). In particular the red and blue wing PFR peaks in Q/I get highly affected in the presence of velocity gradients. We recall that although we have considered a constant velocity field, the Doppler shift $\mu(r, p)V(r)$ along a given impact parameter ray changes (as μ varies due to sphericity effects) thereby producing a velocity gradient in the z-direction. The dependence of I and Q/I profiles on ϵ for non-zero velocity field is similar to the corresponding static case. Apart from producing Doppler shift, the velocity fields modify the source function gradient thereby either enhancing or reducing the anisotropy of the radiation field. In a spherical atmosphere this modification is different for red and blue wing PFR peaks of the Q/I profile (due to sphericity effects and as the intensity is a self-absorbed profile), which results in the high asymmetry noted above. A more detailed discussion can be found in Megha et al. (2019).

4.2 Dependence on continuous absorption parameter β_c

Figure 3 shows the emergent PFR ($I, Q/I$) profiles from a spherically symmetric static (panel a) and a constantly moving atmosphere with $V(r)$=3 (panel b) for varying values of continuous absorption parameter β_c in the range [0, 1]. β_c is the ratio of continuum opacity to frequency averaged line opacity both of which are taken to follow the inverse square law. Hence β_c remains constant throughout the spherical atmosphere. Here the continuum optical depth which is $\beta_c T$ is different for different models. $\beta_c = 0$ corresponds to a pure line case. Here the intensity shows self absorbed emission profile, with the wings falling sharply towards zero due to absence of absorption. With the increase of β_c from 0 to 10^{-6} the intensity does not change much in the line core region but the increase in the value of β_c contributes to the continuum leading to larger values of intensity in the wings. Consequently the emission peaks slowly decrease in their height relative to the continuum and finally cease to exist for $\beta_c = 10^{-4}$, for which the intensity now exhibits an absorption profile. For $\beta_c = 0$, the polarization shows triple peaks due to PFR with highly enhanced wing peaks. The Q/I at the wing PFR peaks is of the order of 50 %. This is because of the strong outward peaking of the radiation field in a spherically symmetric atmosphere, which makes the radiation field highly anisotropic. With the increase in the value of β_c, the magnitude of polarization reduces as the contribution from the unpolarized continuum photons dilute the polarized radiation field. Especially the wing PFR peaks sharply fall down and they disappear for $\beta_c = 10^{-4}$ and with a sign reversal for $\beta_c = 10^{-2}$. This is because the unpolarized continuum source function becomes equal to or larger than the line source function at progressively smaller frequencies (Faurobert 1988, see also Nagendra 1995). For $\beta_c = 1$, the polarization nearly becomes zero with weak negative polarization in the line core. In the presence of velocity field, the intensity for $\beta_c < 10^{-4}$ is strongly affected in the blue region. The effect of velocity field exists only in the line core region of intensity profile with further increase in β_c as the continuum absorption dominates over that of line. The presence of velocity field has similar effects on the polarization profiles with strong enhancement in the magnitude of blue wing PFR peak for $\beta_c < 10^{-4}$.

4.3 Dependence on line averaged radial optical thickness T

Figure 4 shows the emergent PFR ($I, Q/I$) profiles from a spherically symmetric static (panel a) and a constantly moving atmosphere with $V(r)$=3 (panel b) for varying values of optical thickness T from 1 to 10^7. Such a wide variation in T allows us to sample effectively thin ($\epsilon T = 10^{-4}$) to thick ($\epsilon T = 10^3$) atmospheres. The intensity is in emission up to $T = 10^3$ with increasing magnitude and line width. This is clearly an NLTE effect, as number of scatterings increase as T increases. For $T > 10^4$, the medium starts to become effectively thick particularly in the stellar core, thereby giving rise to self absorption in the line core. Thus for T in the range 10^4 to 10^7, the intensity shows self absorbed emission profile with increased broadening. The linear polarization Q/I profiles show a clear sensitivity to variations in T. For T from 1 to 10, the polarization is confined to the line core. This is because the medium is effectively thin ($\epsilon T \ll 1$). With further increase in T from 10^2 to 10^5, PFR wing peaks start to appear with wing peaks shifting towards higher frequency points. Furthermore for $T > 10^3$ the wing PFR peaks exhibit a progressive decrease in magnitude. This outward shift and decrease in magnitude are due to the larger optical depths in the outer layers as the

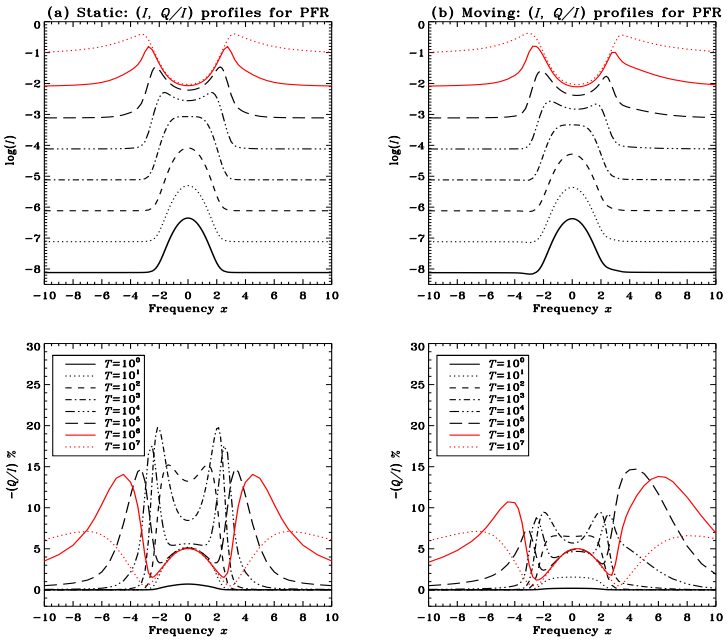

Figure 4. Emergent PFR $(I, Q/I)$ profiles from a spherically symmetric static (panel a) and a constantly moving atmosphere with $V(r)$=3 (panel b) for varying values of line averaged radial optical thickness T (which are given in the inset box).

medium becomes more and more effectively thick with increasing T. For the same reason for $T \geq 10^5$, the central peak is also formed in Q/I. The velocity fields give rise to a Doppler blue shift and also an asymmetry about the line center in the $(I, Q/I)$ profiles. The dependence of I profiles on T for non-zero velocity field is similar to the corresponding static case. For $T \leq 10^4$, the Q/I profiles with velocity fields exhibit a strong Doppler dimming throughout the profile. This is because the corresponding intensity profiles are in emission except for $T = 10^4$. For the same reason the $(I, Q/I)$ profiles are weakly asymmetric about the line center. For $T = 10^4$ a shallow self-absorption in the line core region is seen in I profile. Consequently a slight asymmetry between the red and blue wing PFR peaks in Q/I is seen accompanied with slightly broadened blue wing PFR peak. This asymmetry and broadening of blue wing PFR peak in Q/I are enhanced for $T > 10^4$, as for these cases intensity exhibits a more stronger self-absorption in the line core.

4.4 Dependence on damping parameter a

Figure 5 shows the emergent PFR $(I, Q/I)$ profiles from a spherically symmetric static (panel a) and a constantly moving atmosphere with $V(r)$=3 (panel b) for varying values of damping parameter a in the range 10^{-9} to 10^{-1}. Since we neglect the effects of elastic collisions (namely, $a = \Gamma_R/4\pi\Delta\nu_D$), the variation of a is equivalent to the variation in radiative damp-

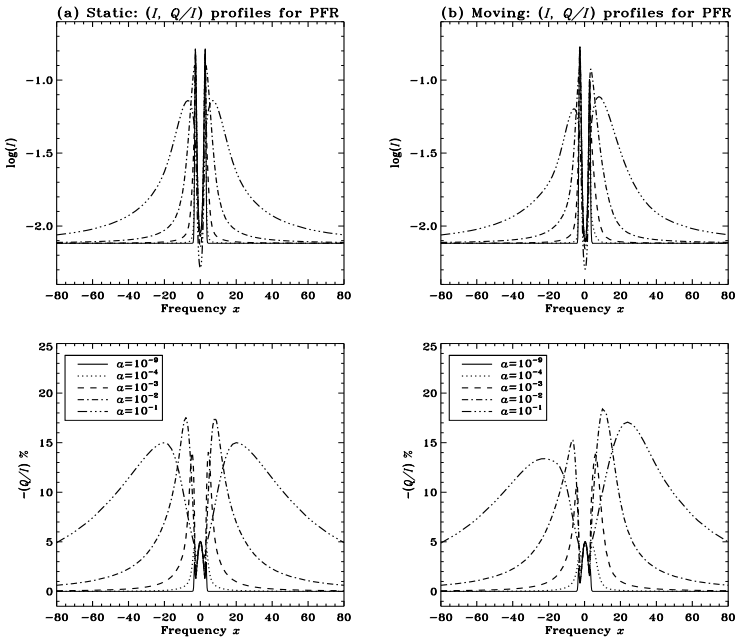

Figure 5. Emergent PFR $(I, Q/I)$ profiles from a spherically symmetric static (panel a) and a constantly moving atmosphere with $V(r)$=3 (panel b) for varying values of damping parameter a (which are given in the inset box).

ing width Γ_R. As the value of a increases intensity profiles become more broader leading to a strong damping wings. The linear polarization profiles also exhibit a broadening with increasing a. In particular the wing PFR peaks are much broader and also shift to larger frequency away from the line center. Moreover, amplitude of wing PFR peaks initially increase with increasing values of a and then decreases for $a = 0.1$ which is perhaps due to excessive line broadening. We recall that with increasing values of a the PFR becomes more and more important resulting in $(I, Q/I)$ profiles shown in Figure 5. This dependence of $(I, Q/I)$ profiles on damping parameter a is similar to the planar case (see e.g., Figure 8 of Sampoorna et al. 2010). In the presence of velocity field the asymmetries are present in $(I, Q/I)$ profiles, while the dependence on variation of a is similar to the corresponding static case.

4.5 Dependence on power law opacity index n

Figure 6 shows the emergent PFR $(I, Q/I)$ profiles from a spherically symmetric static (panel a) and a constantly moving atmosphere with $V(r)$=3 (panel b) for varying values of power law opacity index n. The density distribution in a spherical atmosphere generally obeys a power law type of opacity distribution namely $\chi_{l,c}(r) \propto r^{-n}$. Here we vary n in the range 0 to 4. For $n = 0$, we have a homogeneous sphere. It is well-known that sphericity effects do not develop fully in a homogeneous sphere and are seen only for $n > 1$ (see Kunasz

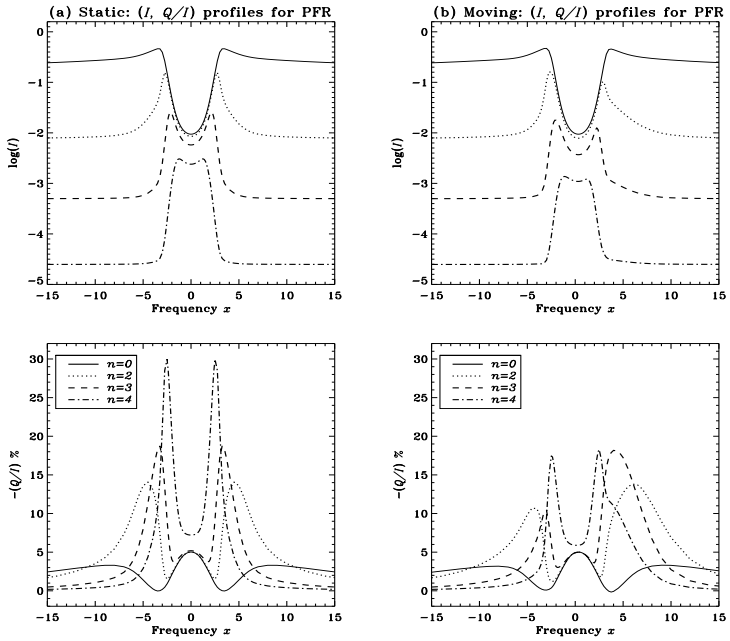

Figure 6. Emergent PFR $(I, Q/I)$ profiles from a spherically symmetric static (panel a) and a constantly moving atmosphere with $V(r)$=3 (panel b) for varying values of power law opacity index n (which are given in the inset box).

& Hummer 1974). Consequently the emission contributions from the extended lobes are uniformly large for $n = 0$ giving rise to an absorption profile in intensity. As n increases the scattering contribution from the extended lobes increases significantly giving rise to self-absorbed emission profile for $n = 2$, 3 and an emission profile with extremely shallow line core absorption for $n = 4$. Since with increasing n, the total opacity rapidly decreases as we move outward, the intensity also drops as n increases. For $n = 0$, 2, and 3 the Q/I profile exhibits a typical triple peak structure. As n increases, the wing PFR peaks become more narrower and shift towards the line core region due to the decrease in optical thickness of extended lobes. Due to dominate contributions from photons that are scattered small number of times, the amplitude of wing PFR peaks also increases with n. For $n \geq 3$ the line core peak disappears as the medium becomes optically thin also at the stellar core. In the presence of velocity field intensity exhibits an asymmetric profile about the line center for $n = 2$, 3, and 4, while the intensity for $n = 0$ exhibits only a blue shift. Even the polarization profiles show asymmetry for $n = 2$, 3, and 4. For $n = 4$ the Q/I exhibits a strong Doppler dimming throughout the profile as the corresponding I profile is nearly in emission.

5 Conclusions

The comoving frame method to solve the problem of polarized PFR line formation in spherically symmetric atmospheres with velocity fields is developed in Megha et al. (2019). Here we use this method to study the effects of different model parameters on the linearly polarized line profiles in spherically symmetric static and moving atmospheres. We have varied the model parameters in a wide range, one at a time, to study their effects on the line profile. We show that the line profiles exhibit a strong dependence on each of the parameters selected for our study and thus help in understanding the polarized lines formed in extended and expanding atmospheres. We show that the velocity fields modify both the amplitude and shape of the Q/I profiles. Such a modification is significant when the corresponding intensity profiles exhibit a self-absorbed emission profile. This is because in this case both Doppler brightening and dimming are simultaneously at play (see Megha et al. 2019 for details). In those cases where the intensity profiles are in emission, the corresponding Q/I profiles exhibit a strong Doppler dimming apart from a Doppler blue shift, when non-zero velocity fields are present in the line forming regions. It is important to note that strong asymmetry between the blue and red wing PFR peaks do not exist if the intensity profiles are in emission or in pure absorption.

Acknowledgements. Megha would like to thank CSIR for the travel grant TG/10856/19-HRD, Indian Institute of Astrophysics and organizers of SPW9 for the partial financial support to participate in the workshop. KNN is thankful to the Director, Indian Institute of Astrophysics for extending the research facilities. KNN also acknowledges the partial support by the organizers of SPW9 and by Dr. M. Bianda, Director, IRSOL that enabled him to participate in the workshop. We acknowledge the use of the high performance computing facility at Indian Institute of Astrophysics.

References

Anusha, L. S., Nagendra, K. N., Paletau, F. & Léger, L. 2009, ApJ, 704, 661
Beals, C. S. 1931, MNRAS, 91, 966
Bommier, V. 1997, A&A, 328, 706
Faurobert, M. 1988, 194, 268
Frisch, H. 2007, A&A, 476, 665
Hauschildt, P. H., & Baron, E. 2004, A&A, 417, 317
Hubeny, I & Mihalas, D. 2014, Theory of Stellar Atmospheres: An Introduction to Astrophysical Non-equilibrium Quantitative Spectroscopic Analysis (Princeton, NJ: Princeton Univ. Press)
Hummer, D. G. & Rybicki, G. B. 1971, MNRAS, 152, 1
Kunasz, P. B. & Hummer, D. G. 1974, MNRAS, 166, 19
Megha, A., Sampoorna, M., Nagendra. K. N., Anusha, L. S., & Sankarasubramanian, K. 2019, ApJ, 879, 48
Nagendra, K. N. 1988, ApJ, 335, 269
— 1994, ApJ, 432, 274
— 1995, MNRAS, 274, 523
— 2003, in ASP Conf. Ser. 288, Stellar Atmosphere Modeling, ed. Hubeny, I., Mihalas, D. & Werner, K., 583
— 2014, in ASP Conf. Ser. 489, Solar Polarization 7, ed. Nagendra, K. N., Stenflo, J. O., Zhongquan Qu & Sampoorna, M. (San Francisco, CA: ASP), 179
Sampoorna, M., Trujillo Bueno, J., & Landi Degl'Innocenti, E. 2010 ApJ, 722, 1269